# Phase Speed Spectra of Transient Eddy Fluxes and Critical Layer Absorption

WILLIAM J. RANDEL

*National Center for Atmospheric Research,* Boulder, Colorado*

ISAAC M. HELD

*Geophysical Fluid Dynamics, Laboratory/NOAA, Princeton, New Jersey*

(Manuscript received 28 March 1990, in final form 15 August 1990)

ABSTRACT

Tropospheric zonal mean eddy fluxes of heat and momentum, and the divergence of the Eliassen–Palm flux, are decomposed into contributions from different zonal phase speeds. Data analyzed are ECMWF operational global analyses covering 1980–87. Eastward moving medium-scale waves (zonal waves 4–7) dominate the spectra of lower tropospheric heat fluxes in both hemispheres and all seasons. Upper tropospheric wave flux spectra are similar to the low level spectra in midlatitudes, but shift to slower zonal phase speeds as low latitudes are approached. The cause of this shift is the selective absorption of faster moving components in midlatitudes as the waves propagate meridionally. Latitude–phase speed distributions of eddy fluxes are constructed and compared to the zonal mean wind structure. These results demonstrate that upper tropospheric eddies break and decelerate the zonal mean flow approximately 10°–20° in latitude away from their critical line (where phase speed equals zonal wind speed). Comparisons are also made with results from the middle stratosphere.

## 1. Introduction

Waves grow baroclinically in midlatitudes and then radiate both vertically and meridionally away from the source region (Edmon et al. 1980; Randel and Stanford 1985). The meridional propagation, which is primarily towards lower latitudes, results in barotropic decay of the waves. Idealized numerical models suggest that irreversible mixing occurs in two distinct regions: 1) in midlatitudes during the growth and occlusion process and 2) at upper levels when the waves break as they propagate into regions of weak mean winds. While it is certainly oversimplified, this picture is useful in suggesting that the eddy flux closure problem might usefully be divided into two parts, corresponding to the two regions of mixing (e.g., Hoskins 1983; Held and Hoskins 1985; Shepherd 1989).

With regard to the wave radiation and barotropic decay phase, one is tempted to rely on linear theory, not only to determine the direction of the radiation but also to predict where the mean flow deceleration associated with the wave breaking and absorption will take place. In particular, linear theory predicts that the distribution of the wave forcing of the mean flow, the Eliassen–Palm (E–P) flux divergence, is strongly constrained by the space–time spectrum of the disturbance emanating from the source region: that part of the disturbance's wave activity, or pseudomomentum, characterized by phase speeds between $c$ and $c + \delta c$ will be deposited where the mean zonal flow $\bar{u}$ satisfies $c < \bar{u} < c + \delta c$. See Held and Phillipps (1987) for a simple barotropic example of wave radiation and decay analyzed in this way.

Finite-amplitude disturbances decelerate the flow in more complex ways, as also illustrated in the barotropic example of Held and Phillipps and in a number of baroclinic wave propagation studies, many of which have focused on the stratosphere and the sudden warming phenomenon (Robinson 1988; O'Neill and Pope 1988 are two recent examples). If the disturbance has a relatively well-defined phase speed, linear theory predicts that the E–P flux divergence will be localized in narrow "critical" layers, but as the meridional particle displacements generated by the wave in the breaking region grow, the E–P flux divergence must be expected to spread over a wider region spanned by these displacements. On this basis, one is led to expect that a smeared out version of the linear prediction might be relevant. But it is also found in idealized calculations that finite-amplitude waves generally break before they reach their critical latitude (see also in this regard the two-layer life cycle study of Feldstein and Held 1989), so that the pseudomomentum is deposited at latitudes

* The National Center for Atmospheric Research is sponsored by the National Science Foundation.

*Corresponding author address:* Dr. William Randel, NCAR, P.O. Box 3000, Boulder, CO 80307.

where the zonal flow is still substantially larger than the phase speed. Large dissipation would have a qualitatively similar effect on the distribution of the drag, preventing the spatial separation between the source region and the region of drag deposition from being as large as predicted by inviscid linear theory. Intuitively, "wave–wave interactions," or the mixing induced by the breaking of other waves in the spectrum, could play such a dissipative role.

In this paper we test these expectations against observations by examining the phase speed spectra (more generally, the wavenumber–phase speed spectra) of the tropospheric eddy heat and momentum fluxes, and the E–P flux divergence, as functions of latitude and height. We compare these spectra in the different seasons and hemispheres. Additionally, we present results for eddies in the winter stratosphere of both hemispheres. Space–time energy spectra are a common starting point for many studies (Hayashi 1982). Space–time cospectra of tropospheric heat and momentum fluxes have been given surprisingly little attention. Mechoso and Hartman (1982) present heat and momentum flux covariance spectra for high southern latitudes during May-September 1979, with a focus on planetary wave characteristics. Zangvil and Yanai (1980) and Yanai and Lu (1983) compute space–time spectra of the momentum flux in the low-latitude upper troposphere, with the purpose of studying the sources of equatorial waves. Our primary focus in this study is on the location of the wave absorption regions in the upper troposphere as a function of phase speed.

## 2. Data and analyses

### a. Data

The tropospheric data utilized here are daily global analyses of winds and temperatures from the European Centre for Medium Range Weather Forecasts (ECMWF), covering the years 1980–87. Data are available on seven standard pressure levels (1000, 850, 700, 500, 300, 200 and 100 mb), with the original archive consisting of 2.5 × 2.5 degree latitude–longitude grids. These grids have been converted to 7.5 by (approximately) 4.5 degree longitude–latitude grids, consistent with rhomboidal spectra truncation at wavenumber 15, and archived at NCAR. These data have subsequently been used to calculate zonal Fourier coefficients up to wavenumber 12 on the (approximate 4.5 degree) Gaussian latitude grid, and these form the basis of the analyses here. An extensive discussion of the ECMWF data and assessment of its quality can be found in Trenberth and Olson (1988). Time series of length 120 days are analyzed during Northern Hemisphere (NH) winter (December–March, hereafter DJFM), and Southern Hemisphere (SH) winter (June–September, JJAS), and the spectra are averaged appropriately over the available years of data.

We also present results for winter transient eddies in the middle stratosphere. The data used in these calculations are based on linear balance winds and hydrostatic temperatures derived from stratospheric geopotential height data produced operationally at the National Meteorological Center/Climate Analysis Center. Details of the data and wind derivations can be found in Randel (1987). Spectra presented are four year averages (1985–88) calculated from 120-day time series during NH and SH winter.

### b. Spectral analyses

Space–time cross-spectral analyses are used here to characterize the disturbances that contribute to the zonal mean eddy fluxes. For any two longitude–time series $a(\lambda, t)$ and $b(\lambda, t)$, the estimate of the space–time cospectra power density is defined as

$$K_{n,\omega}(a, b) = 2\langle \mathrm{Re}(A_{n,\omega}B^*_{n,\omega})\rangle, \qquad (1a)$$

where the angle brackets represent averaging over a frequency bandwidth needed to obtain a spectral estimate from a finite time series (and over different realizations of the time series), and

$$A_{n,\omega} = \frac{1}{2\pi T}\int_0^T dt \int_0^{2\pi} a(\lambda, t)e^{-i(n\lambda+\omega t)}d\lambda \qquad (1b)$$

(and similarly for $B_{n,\omega}$). Here $n$ is the number of waves fitting around a latitude circle. Using the convention that $n$ is positive, positive and negative $\omega$ correspond to westward and eastward propagation, respectively. We follow the method described in Hayashi (1971, his Eq. 4–11) for the computation of $K_{n,\omega}$. Time spectra are calculated by direct Fourier transform, and smoothed at frequency $\omega_0$ using a normalized Gaussian spectral window of the form

$$W(\omega - \omega_0) = e^{-[(\omega-\omega_0)/\Delta\omega]^2}, \qquad (2)$$

with $\Delta\omega = 3$. This choice of spectral window was chosen to give a good balance between spectral resolution and stability. Figure 1a shows an example wavenumber–frequency contour diagram for transient eddy poleward heat flux ($\overline{v'T'}$) at 300 mb, 47°N during DJFM, showing strong covariance for eastward propagating zonal waves 4–7.

Wavenumber–phase speed ($c$) spectra are calculated as follows. The spectral power density in phase speed space is defined so that total power is conserved in the transformation from frequency space, i.e.,

$$K_{n,c} \cdot \Delta c = K_{n,\omega} \cdot \Delta\omega. \qquad (3a)$$

Since $\omega = c(n/a\cos\phi)$, we get

$$K_{n,c} = K_{k,\omega} \cdot \left(\frac{n}{a\cos\phi}\right). \qquad (3b)$$

The $K_{n,c}$ is calculated by constructing a phase speed grid (of resolution 1 m s$^{-1}$), and interpolating the

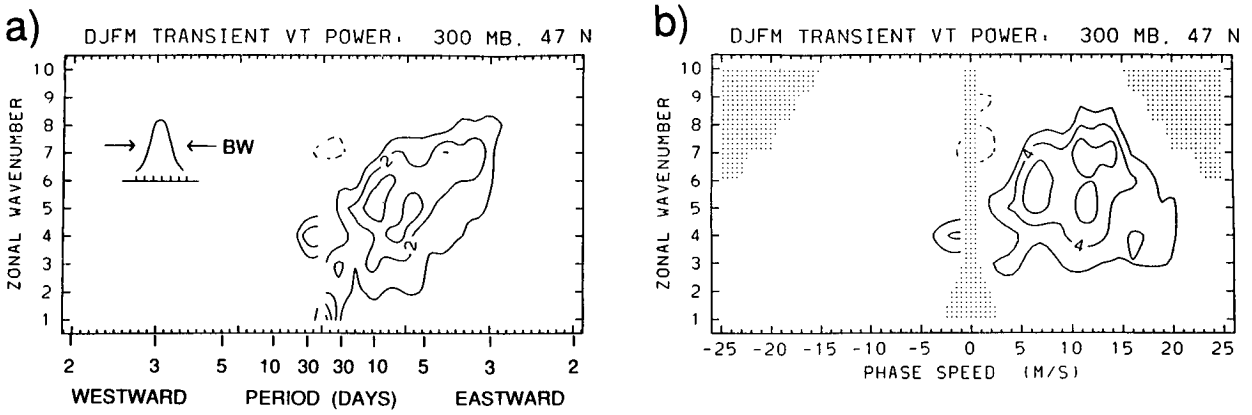


FIG. 1. Zonal wavenumber–frequency covariance spectra of $\overline{v'T'}$ at 300 mb, 47°N during DJFM. The spectral bandwidth (BW) associated with the Gaussian spectral window (2) is also shown. Spectral density contour interval is 0.01 K m s$^{-1}$ · $\Delta\omega^{-1}$, with $\Delta\omega$ the unit frequency interval of ($2\pi$/120 days). (b) Zonal wavenumber phase speed covariance spectra calculated from (a) via (3). Contour interval is 0.02 K m s$^{-1}$ · $\Delta c^{-1}$, with $\Delta c$ the unit phase speed interval of 1.0 m s$^{-1}$. Shaded regions denote wavenumber–phase speed combinations which are unresolved at this latitude (as discussed in text).

spectral density at each phase speed from the two closest frequency estimates of $K_{n,\omega}$, then multiplying by ($n$/$a\cos\phi$). The sum of the covariance is then essentially the same whether summed in frequency or phase speed space.

Figure 1b shows a wavenumber–phase speed diagram constructed from the data in Fig. 1a. Note the relative increase in spectral density for higher zonal wavenumbers as compared to Fig. 1a, due to the $n$ factor in (3b). A point to note is that, due to the frequency limits imposed by 120-day time series ($\omega_{low}$ = $2\pi$/120 days, $\omega_{high}$ = $2\pi$/2 days), some wavenumber–phase speed combinations are unresolved in these data. For example, for zonal wave 1, the lowest phase speed resolvable at 47°N is $c_{low}$ = 2.6 m s$^{-1}$, while for wave 10, $c_{high}$ = 15.8 m s$^{-1}$. Regions where the power is unresolved are shaded in Fig. 1b and the following wavenumber–phase speed diagrams. Because the lowest phase speeds are unresolved, the tropospheric latitude–phase speed diagrams (section 4) show spectra only for (absolute values of) phase speeds greater than or equal to 2 m s$^{-1}$.

One could also choose to consider the spectral density as a function of angular phase speed, $\omega/n$, rather than $c$, motivated by the fact that $\omega$ and $n$ are both conserved as a wavepacket propagates meridionally through a time-independent, zonally symmetric flow. Since we will be comparing the spectra to the zonal wind distribution, we have chosen to work with $c = \omega a\cos\phi/n$ rather than $\omega/n$.

### 3. Wavenumber–phase speed spectra

Figure 2 shows a series of wavenumber–phase speed spectra for transient eddy poleward heat flux at 700 mb, 47°N and S, for DJFM and JJAS. This is near the location of maximum transient heat flux for each season. Also added in the right hand panels of Fig. 2 are the summed contribution from all transients (dashed lines) and stationary waves (solid lines), plotted as a function of zonal wavenumber. Here stationary refers to the time mean components, not waves with fluctuating amplitudes and zero phase speed. These figures demonstrate several familiar facts:

1) Transient wave heat flux is dominant in all seasons except NH winter, where stationary planetary wave ($n$ = 1–3) fluxes are equally important.

2) Transient wave heat fluxes are maximum for medium-scale waves ($n$ = 4–7, zonal wavelengths ≈ 4–7000 km) moving eastward with phase speeds of order 5–15 m s$^{-1}$.

3) The phase speed spectra show an overall slope of the contours, such that higher wavenumbers (shorter zonal scales) move with successively faster eastward phase speeds.

4) The NH spectra are somewhat broader in wavenumber decomposition, suggesting the importance of spatially localized features. Conversely, the more concentrated SH spectra (especially during SH summer) show the importance of medium scale waves of hemispheric extent (such as the global wave 5 features discussed by Salby 1982; Hamilton 1983; Randel and Stanford 1985).

The predominance of eastward moving medium scale waves seen in Fig. 2 is also observed for other cross spectra throughout the midlatitude troposphere. Similar signatures are observed for eddy momentum flux (shown below), transient eddy kinetic energy (not shown here), and upper tropospheric geopotential height fluctuations (Bottger and Fraedrich 1980; Fraedrich and Kietzig 1983; Speth and Madden 1983). Similar spectra are also found in general circulation model results (e.g., Hayashi and Golder 1977).

As waves propagate towards low latitudes in the up-

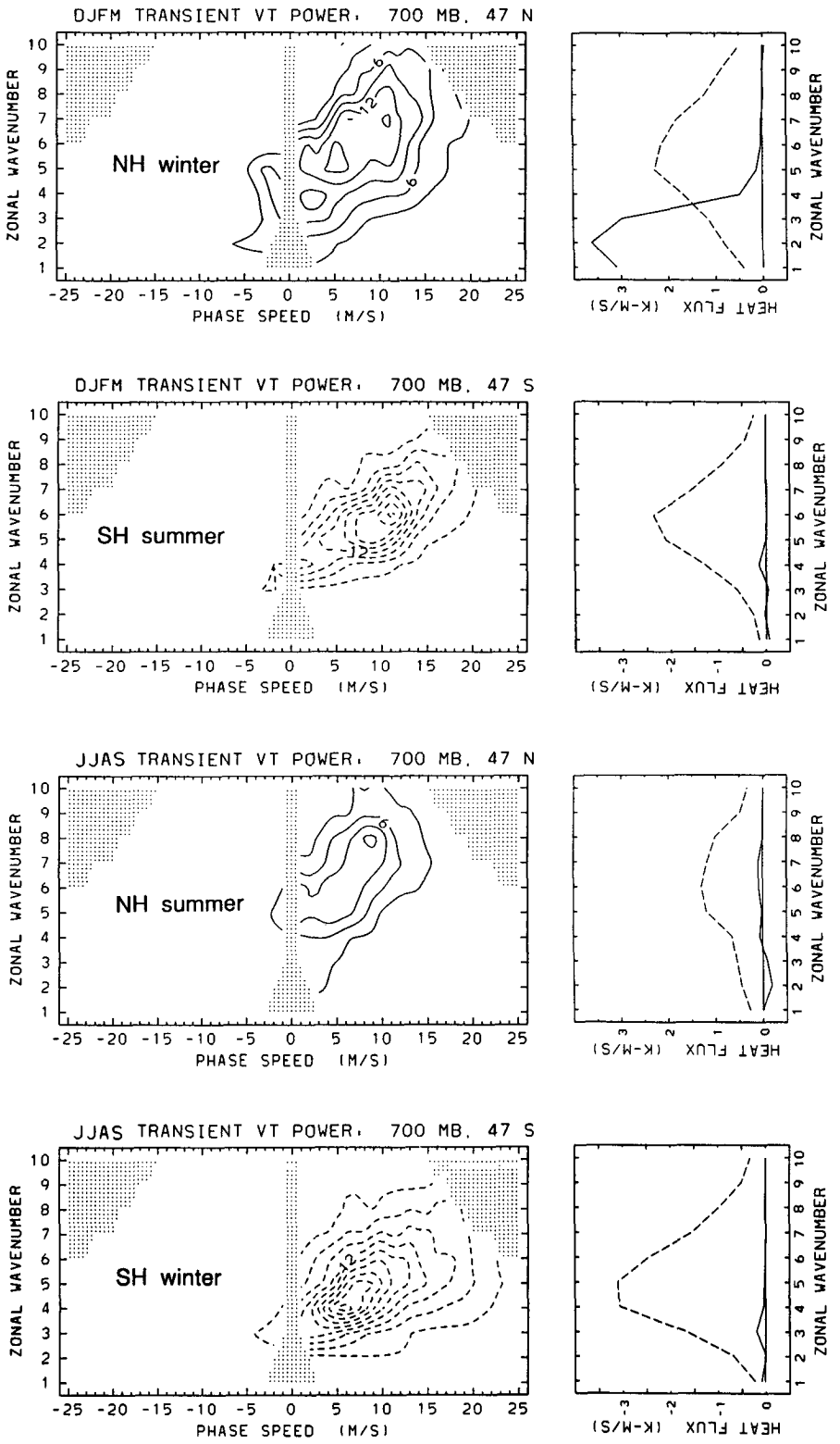


FIG. 2. Left panels show wavenumber–phase speed covariance spectra for midlatitude (47°) low level (700 mb) heat flux, for NH and SH summer and winter statistics (as labeled). Contour interval is 0.03 K m $s^{-1} \cdot \Delta c^{-1}$. Right panels show total transient (dashed lines) and stationary (solid lines) contribution to poleward heat flux versus wavenumber for each location and season, illustrating the relative importance of transient and stationary contributions.

per troposphere, the higher phase speed components are selectively removed from the spectra. Figure 3 shows eddy momentum flux cospectra at 38° (near the latitude of maximum flux) and at 20° for NH and SH winters. The spectra at 38° show patterns similar to the respective heat flux signatures in Fig. 2. The spectra at 20° show similarly positioned spectral peaks for the lowest phase speeds (near $n = 6$, $c \sim 5$ m s$^{-1}$ for NH and $n = 4$, $c \sim 7$ m s$^{-1}$ for SH), while much of the higher phase speed covariance at 38° is absent at 20°; this suggests that the faster waves are preferentially absorbed before they reach the subtropics.

A concise measure of the eddy forcing of the zonal mean flow, and, if the dynamics is approximately linear, of nonconservative wave effects, is provided by the divergence of the E–P flux (Edmon et al 1980). Figure 4 shows wavenumber–phase speed spectra of the quasi-geostrophic E–P flux divergence $D_F$ multiplied by cosine of latitude in the midlatitude middle troposphere (47°S, 500 mb) and in the subtropical upper troposphere (24°S, 200 mb) during SH winter. $D_F$ is calculated from:

$$D_F = \frac{1}{a\cos^2\phi}\frac{\partial}{\partial\phi}(-\overline{u'v'}\cos^2\phi) + \rho_s^{-1}\frac{\partial}{\partial z}\left(\rho_s f\frac{\overline{v'T'}}{N^2}\right), \quad (4)$$

with $\rho_s$ the background density and $N^2$ the (latitude–height dependent) static stability parameters, respectively. We include the $\cos\phi$ factor so as to have a measure of the torque exerted by the eddies on the mean flow. Spectral components of $D_F$ were calculated directly from spectra of $\overline{u'v'}$ (as in Fig. 3) and $\overline{v'T'}$ (as in Fig. 2). The positions chosen in Fig. 4 represent two contrasting regions of baroclinic wave activity, both where the eddies exert a drag on the mean flow. Spectra at 47°, 500 mb (Fig. 4a) are directly above the storm track region in the middle troposphere; $D_F$ here is a result of the opposing effects of the momentum and heat flux terms in (4). The latter is the dominant term, and the $D_F$ spectra are shaped similarly to the heat flux spectra in Fig. 2. The subtropical upper tropospheric $D_F$ spectrum (Fig. 4b) primarily results from the convergence of momentum flux, as can be seen by comparison with the SH winter $\overline{u'v'}$ spectra in Fig. 3 (the 24° $D_F$ spectra is approximately the difference between the 38° and 20° spectra in Fig. 3).

## 4. Latitudinal structure of phase speed spectra

The idealized model studies discussed in the Introduction suggest that the latitudinal dependence of the eddy flux phase speed spectra should be related to the horizontal structure of the zonal mean flow. A concise way to look for such a dependence is to sum the con-

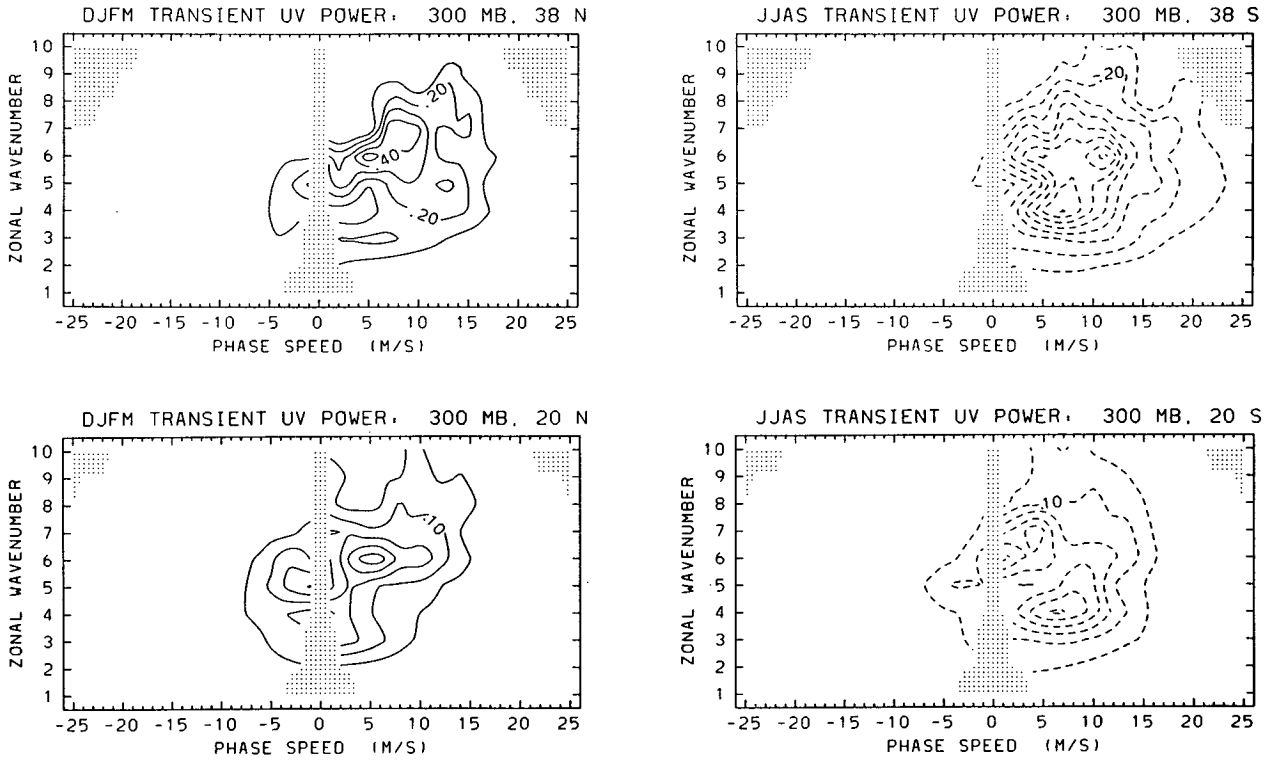


FIG. 3. Zonal wavenumber–phase speed spectra for transient eddy momentum flux at 38° (top) and 20° (bottom), for NH winter (left) and SH winter statistics (right). Contour interval is 0.10 m$^2$ s$^{-2}\cdot\Delta c^{-1}$ in the upper and 0.05 m$^2$ s$^{-2}\cdot\Delta c^{-1}$ in the lower panels.

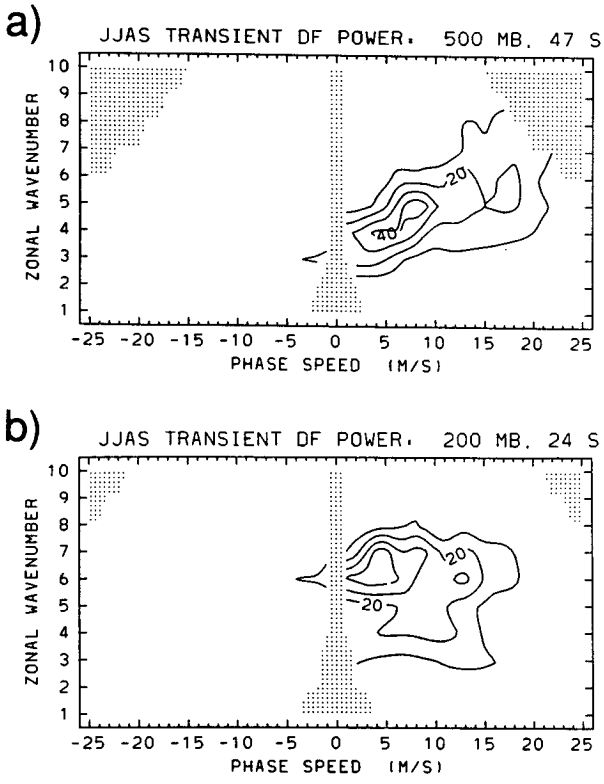


FIG. 4. Zonal wavenumber phase speed spectra of transient wave EP flux divergence $D_F$ (4) multiplied by cosine of latitude at 300 mb, (a) 47°S and (b) 29°S for SH winter statistics. The sign of $D_F$ has been reversed to agree with Fig. 7, i.e., positive contours denote negative $D_F$. Contour interval is 0.01 m s$^{-1}$ per day · $\Delta c^{-1}$.

tributions from all zonal wavenumbers, and plot contour diagrams of wave covariance versus latitude and phase speed. Figure 5 shows such diagrams for 700 mb heat flux, for DJFM and JJAS. These diagrams define the spectra of low-level baroclinic wave generation, along with its seasonal and hemispheric dependence. The patterns show broad maxima in middle to high latitudes, spanning a range of eastward phase speeds of order 0–20 m s$^{-1}$. The latitudinal extent of $\overline{v'T'}$ changes seasonally in both hemispheres, with winter maxima approximately 10° equatorward of those in summer. Northern Hemisphere fluxes exhibit eastward maxima near 5–10 m s$^{-1}$, along with high latitude quasi-stationary covariance, especially in winter. Southern Hemisphere patterns in Fig. 5 show maxima near 10 and 6 m s$^{-1}$ in DJFM and JJAS, respectively.

Figure 6 shows latitude–phase speed diagrams for 300 mb transient eddy momentum flux, a signature of meridional wave propagation. Southern Hemisphere patterns in Fig. 6 show equatorward propagation (poleward momentum flux) equatorward of 55°S, and poleward propagation south of this latitude, signifying a divergence of wave activity from midlatitudes. Northern Hemisphere transient wave propagation is almost entirely equatorward. This is an important difference between the two hemispheres, which appears in both seasons. Comparisons of Figs. 5–6 shows a nearly one-to-one correspondence between the phase speed of maxima in $\overline{u'v'}$ and of maxima in $\overline{v'T'}$.

Figure 6 also includes lines indicating the seasonal mean 300 mb zonal mean zonal wind $\bar{u}$ in each diagram and shading which denotes plus and minus one daily standard deviation in $\bar{u}$. Linear theory predicts that waves will not propagate meridionally beyond their critical line, where $\bar{u} = c$; in Fig. 6 this would show up as an absence of $\overline{u'v'}$ at phase speeds faster than $\bar{u}$. There is excellent agreement with this prediction in both hemispheres and both seasons. The fastest phase

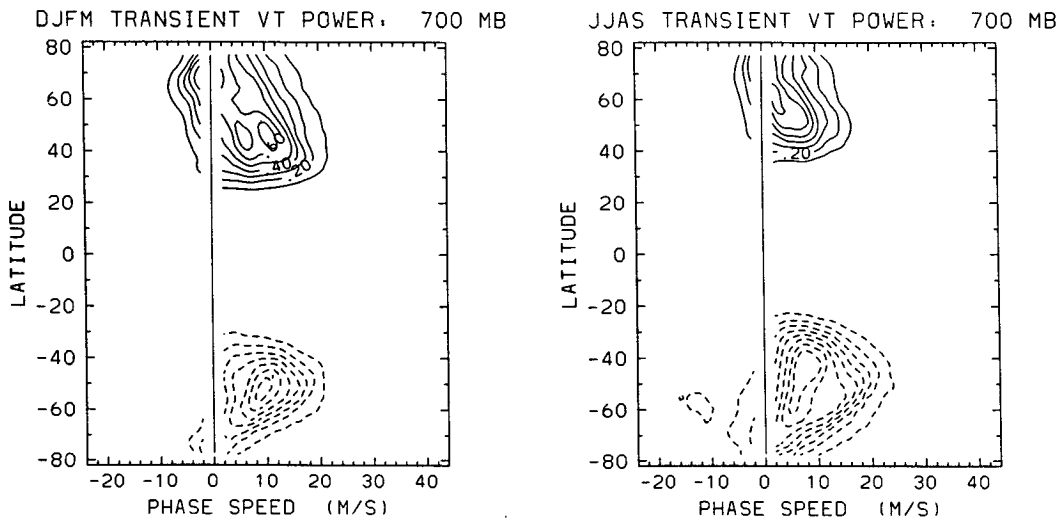


FIG. 5. Contours of 700 mb transient eddy heat flux versus latitude and phase speed for DJFM (left) and JJAS (right). Contour interval is 0.10 K m s$^{-1}$ · $\Delta c^{-1}$.

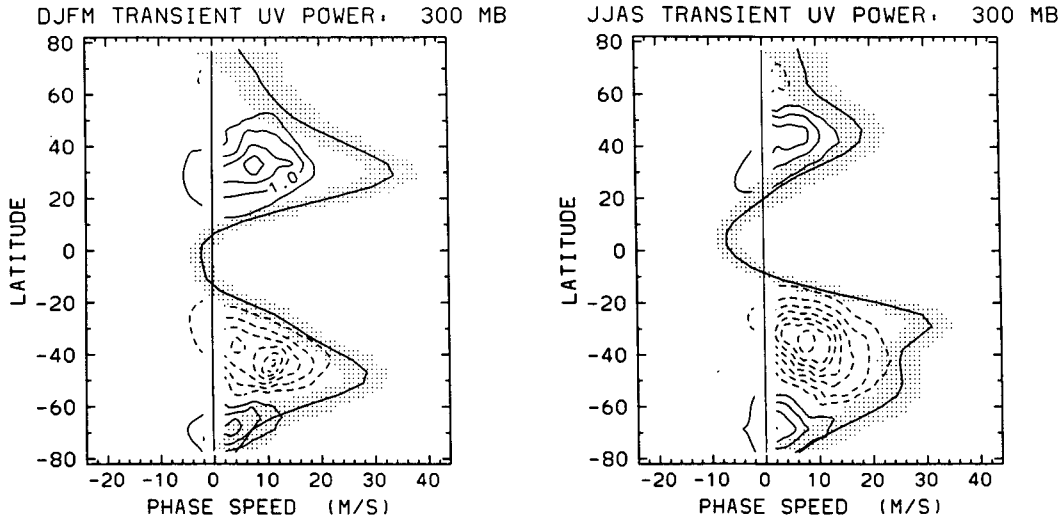


FIG. 6. Contours of 300 mb transient eddy momentum flux versus latitude and phase speed for DJFM (left) and JJAS (right). Contour interval is 0.50 $m^2\ s^2 \cdot \Delta c^{-1}$, with zero contours omitted. Heavy lines in each panel denote seasonal average zonal mean zonal wind, and shading denotes plus and minus one daily standard deviation.

speeds are confined near the respective jet cores, and waves with smaller phase speeds propagate more deeply into the tropics. This is particularly clear in the SH summer, where the covariance isolines in the subtropics are nearly parallel to the zonal wind profile.

Similar plots for the divergence of the EP flux are shown in Fig. 7 for the 500, 300 and 200 mb levels. Again we have multiplied $D_F$ by $\cos\phi$ so as to be proportional to the torque exerted by the eddies on the mean flow. The middle tropospheric (500 mb) patterns show wave drag concentrated in middle and high latitudes, with a majority directly above the wave generation regions identified in Fig. 5. These maxima result primarily from the vertical convergence term in (4). At 200 mb the wave drag is located almost exclusively in the subtropics, this being the result of the equatorward wave propagation from midlatitudes. The 300 mb level shows patterns midway between those at 500 and 200 mb. The simplest picture of linear wave radiation on a steady zonal flow predicts that the power in the subtropical upper troposphere should be aligned along the $\bar{u} = c$ curve. Figure 7 shows maxima in $D_F$ approximately 10°–20° latitude away from the respective critical lines for each season. This distance in latitude is roughly consistent between the seasons, whereas the velocity difference between the maximum in $D_F$ and $\bar{u}$ at that latitude is not constant (compare the difference at 40°S in SH summer, $\sim 10\ m\ s^{-1}$, with that at 30° in SH winter, $\sim 20\ m\ s^{-1}$). This suggests that meridional displacement from the critical latitude is more relevant for the drag deposition than is $(\bar{u} - c)$. The distance from the critical latitude at which breaking occurs should be related to the eddy energy level, but we have not found a simple quantitative argument for the observed displacement.

A minimum in $D_F$ at the latitude of the maximum in the lower tropospheric eddy heat flux (Fig. 5) is clear in Fig. 7 at 300 and 200 mb. Since $D_F$ is associated with irreversible mixing (e.g., Edmon et al. 1980), the implication is that the bulk of the *upper* tropospheric mixing is located well north and south of the storm track, with the flow immediately above the storm track more nearly conservative. In the *middle* troposphere, mixing is largest above and poleward of the storm tracks. This picture is consistent with the numerical life cycle studies of Simmons and Hoskins (1978).

Figure 8 shows latitude–phase speed distributions of EP flux divergence for the middle stratosphere (10 mb). An important point to note is that because low-frequency planetary waves (zonal waves 1–2) dominate much of the stratospheric spectra (not shown here), there is a substantial amount of covariance at low phase speeds that is unresolved in these analyses (cf. Fig. 1b and discussion in section 2b). Figure 8 therefore shows spectra only for (absolute values of) phase speeds greater than or equal to $4\ m\ s^{-1}$. This unresolved covariance is particularly large in the NH winter where planetary waves are often quasi-stationary; there it accounts for approximately 45% of the total (area averaged) transient $D_F$ variance. In the SH winter planetary waves propagate more regularly eastward, and only 15% of the transient $D_F$ variance is unresolved in our analyses.

The NH winter patterns in Fig. 8a show the quasi-stationary $D_F$ activity as slow eastward and westward maxima centered near 35°N. This is approximately 20°–30° in latitude poleward of the near-zero wind line in the tropics. Southern Hemisphere winter statistics (Fig. 8b) show eastward propagating covariance in the range 0–20 $m\ s^{-1}$, with notable alignment of the

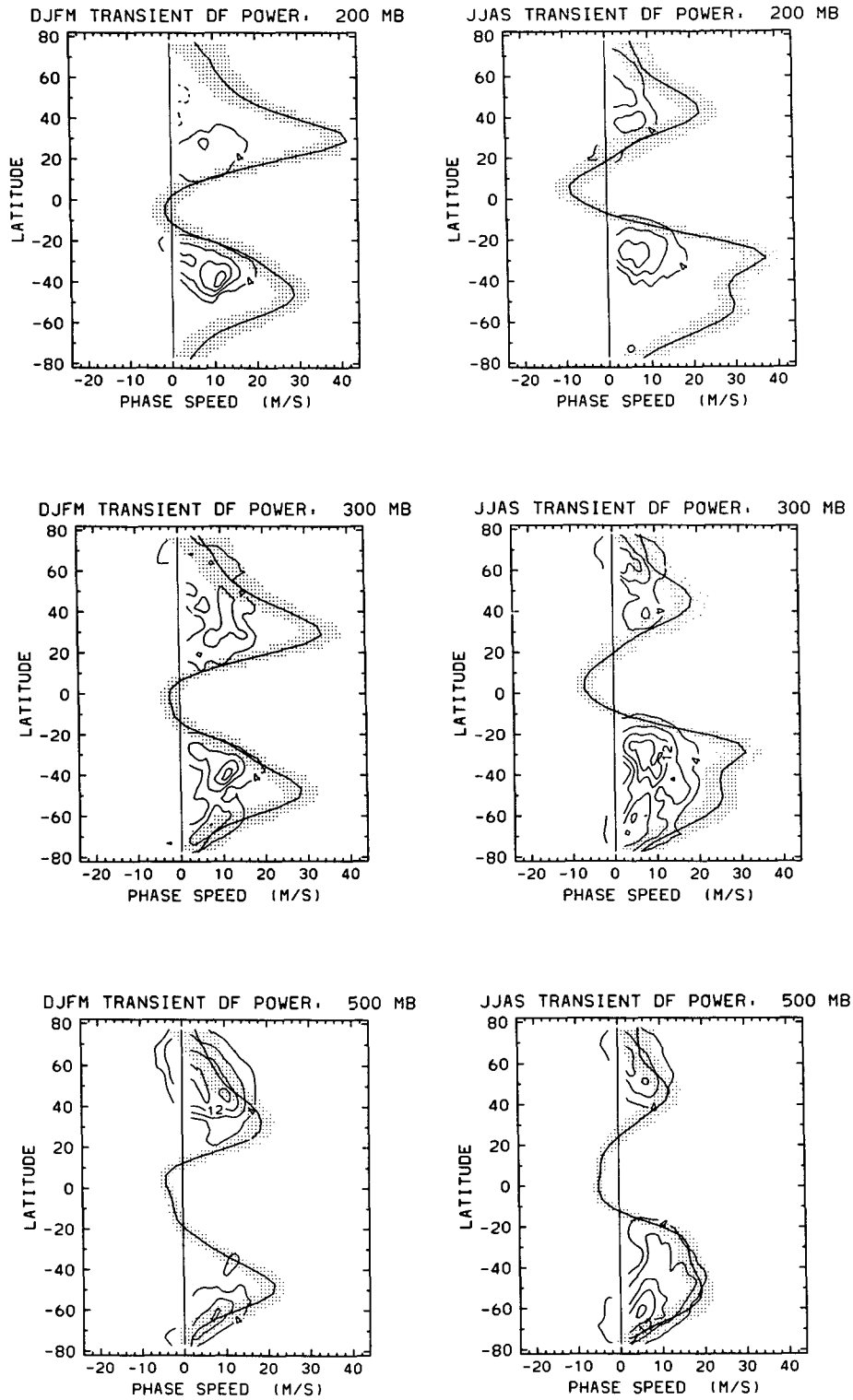


FIG. 7 Contours of transient wave EP flux divergence [$D_F$, Eq. (4)], multiplied by cosine of latitude, at 500 mb (lower), 300 mb (middle) and 200 mb (top). For clarity the sign of $D_F$ has been reversed, i.e., solid lines denote negative $D_F$. Contour interval is 0.04 m s$^{-1}$ per day $\cdot$ $\Delta c^{-1}$. Heavy lines in each panel denote seasonal average zonal mean zonal wind, and shading denotes plus and minus one daily standard deviation.

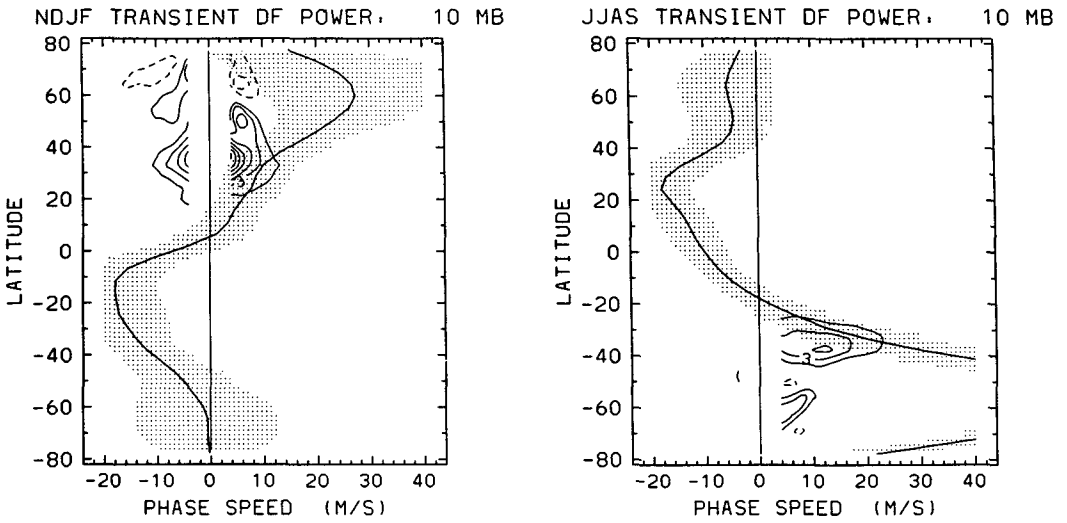


FIG. 8. Latitude–phase speed spectra of $D_F \cos\phi$ for circulation statistics in the middle stratosphere (10 mb). Left panel shows NH winter statistics (November–February), right panel SH winter data (June–September). Contour interval is 0.015 m s$^{-1}$ per day $\cdot$ $\Delta c^{-1}$, with zero contours omitted. Note that due to sampling considerations, contours are only drawn for (absolute values of) phase speeds greater than or equal to 4 m s$^{-1}$ (see text for discussion). Heavy lines in each panel denote zonal mean zonal wind, and shading denotes plus and minus one daily standard deviation.

$D_F$ contours in the subtropics, parallel to and approximately 10° in latitude poleward of the critical line. This closer approach to the critical line in the SH winter may be due to significantly smaller amplitude waves in the SH, and hence a closer approximation to linear wave behavior.

## 5. Concluding remarks

While the dominant eddies in the troposphere are certainly "turbulent" in some sense, they also retain some wavelike characteristics. To test the importance of these wavelike characteristics for the structure of the eddy fluxes, we decompose these fluxes into contributions from different zonal phase speeds. The momentum flux and E–P flux divergence cospectra demonstrate that wavelike properties are indeed strong enough to influence the interaction between the eddies and the mean flow.

Upper tropospheric eddies of phase speed $c$ propagate away from their source region, where $\bar{u}$ is much larger than $c$, into regions of smaller $(\bar{u} - c)$ north and south of the source. The observations here demonstrate a clear tendency for eddies of smaller zonal phase speed to propagate further into regions of smaller $\bar{u}$. The eddies typically do not reach their critical latitudes. Largest pseudomomentum deposition is found 10°–20° latitude from the wave's critical latitude. Here they mix the potential vorticity and decelerate the mean flow. The mixing and the associated drag on the mean flow are relatively small in the upper troposphere above the source region itself. That the flow is more nearly conservative immediately above the storm track is counterintuitive but consistent with numerical models of baroclinic eddy life cycles. These results lend some support to eddy flux closure schemes in which the problem is split into two parts: a theory for the space–time spectrum of the wave activity propagating into the upper troposphere (i.e., of the lower tropospheric heat flux) and a theory that accounts for the meridional propagation of these eddies on the upper tropospheric flow and the resulting wave breaking and mixing that determine the pattern of the mean flow deceleration.

The approximation of setting the drag equal to zero everywhere except along the $\bar{u} = c$ line is not quantitatively accurate; this study suggests that a more useful approximation may be to spread the drag over a region 10°–20° from the critical latitude. This distance is presumably controlled by the amplitude of the eddies. Even after making this gross simplification, one would still need some way of determining how much of the wave activity was deposited north and how much south of the source.

Data for the SH show the strongest localized maxima and minima in $D_F$ in the upper troposphere. The picture is somewhat less clear in the Northern Hemisphere, and this may be attributable to the NH storm tracks and time-mean flow being distributed more asymmetrically in longitude than their SH counterparts. It is possible that cleaner results, with a "conservative" upper troposphere directly above the storm track, surrounded by regions of drag deposition to the north and south, would be obtained by focusing on certain regions. But it is also plausible that substantial irreversible mixing occurs in the upper troposphere at the latitude of the storm track when the track is strongly zonally

asymmetric, particularly in the barotropic decay regions that are favorable for blocking (Shutts 1983), and that this mixing cannot be understood even qualitatively in terms of waves propagating on zonal flows.

*Acknowledgments.* This work was initiated while both authors were visitors to the Climate and Global Dynamics division at NCAR. We thank Yoshikazu Hayashi, Kevin Trenberth, Joe Tribbia and the anonymous reviewers for suggestions on the manuscript. The tropospheric data analyzed here were provided by ECMWF. WJR has been partially supported under NASA Grant W-16215.

## REFERENCES

Bottger, H., and K. Fraedrich, 1980: Disturbances in the wavenumber–frequency domain observed along 50°N, *Contrib. Atmos. Physics,* **53,** 90–105.

Edmon, H. J. Jr., B. J. Hoskins and M. E. McIntyre, 1980: Eliassen–Palm cross sections for the troposphere. *J. Atmos. Sci.,* **37,** 2600–2616; also Corrigendum, *J. Atmos. Sci.,* **38,** 1115 (1981).

Feldstein, S., and I. M. Held, 1989: Barotropic decay of baroclinic waves in a two-layer beta-plane model. *J. Atmos. Sci.,* **46,** 3416–3430.

Fraedrich, K., and E. Kietzig, 1983: Statistical analysis and wavenumber–frequency spectra of the 500 mb geopotential along 50°S. *J. Atmos. Sci.,* **40,** 1037–1045.

Hamilton, K., 1983: Aspects of wave behavior in the mid and upper troposphere of the Southern Hemisphere. *Atmos. Oceans,* **21,** 40–54.

Held, I. M., and B. J. Hoskins, 1985: Large-scale eddies and the general circulation of the troposphere. *Advances in Geophysics,* **28A,** Academic Press, 3–31.

——, and P. J. Phipps, 1987: Linear and nonlinear barotropic decay on the sphere. *J. Atmos. Sci.,* **44,** 200–207.

Hayashi, Y., 1971: A generalized method of resolving disturbances into progressive and retrogressive waves by space Fourier and time cross-spectral analyses. *J. Meteor. Soc. Japan,* **49,** 125–128.

——, 1982: Space–time spectral analysis and its applications to atmospheric waves. *J. Meteor. Soc. Japan,* **60,** 156–171.

——, and D. G. Golder, 1977: Space–time spectral analysis of mid-latitude disturbances appearing in a GFDL general circulation model. *J. Atmos. Sci.,* **34,** 237–262.

Hoskins, B. J., 1983: Modelling of the transient eddies and their feedback on the mean flow. *Large Scale Dynamical Processes in the Atmosphere,* B. J. Hoskins and R. P. Pearce, Eds., Academic Press, 397 pp.

Mechoso, C. R., and D. L. Hartmann, 1982: An observational study of traveling planetary waves in the Southern Hemisphere. *J. Atmos. Sci.,* **39,** 1921–1935.

O'Neill, A., and V. Pope, 1988: Simulations of linear and nonlinear disturbances in the stratosphere. *Quart. J. Roy. Meteor. Soc.,* **114,** 1063–1110.

Randel, W. J., 1987: Global atmospheric circulation statistics, 1000–1 mb. NCAR Tech. Note, NCAR/TN-295+STR, 245 pp.

——, and J. L. Stanford, 1985: The observed life cycle of a baroclinic instability. *J. Atmos. Sci.,* **42,** 1364–1373.

Robinson, W. A., 1988: Irreversible wave–mean flow interactions in a mechanistic model of the stratosphere. *J. Atmos. Sci.,* **45,** 3413–3430.

Salby, M., 1982: A ubiquitous wave 5 anomaly in the Southern Hemisphere during FGGE. *Mon. Wea. Rev.,* **110,** 1712–1720.

Shepherd, T. G., 1989: Nonlinear saturation of baroclinic instability. Part II: Continuously stratified fluid. *J. Atmos. Sci.,* **46,** 888–907.

Shutts, G. J., 1983: The propagation of eddies in diffluent jet streams: Eddy vorticity forcing of blocking flow fields. *Quart. J. Roy. Meteor. Soc.,* **109,** 737–761.

Simmons, A. J., and B. J. Hoskins, 1978: The life cycles of some non-linear baroclinic waves. *J. Atmos. Sci.,* **35,** 414–432.

Speth, P., and R. A. Madden, 1983: Space–time spectral analyses of Northern Hemisphere geopotential heights. *J. Atmos. Sci.,* **40,** 1086–1100.

Trenberth, K. E., and J. G. Olson, 1988: An evaluation and intercomparison of global analyses from the National Meteorological Center and the European Centre for Medium Range Weather Forecasts. *Bull. Amer. Meteor. Soc.,* **69,** 1047–1057.

Yanai, M., and M.-M. Lu, 1983: Equatorially trapped waves at the 200 mb level and their association with meridional convergence of wave energy flux. *J. Atmos. Sci.,* **40,** 2785–2803.

Zangvil, A., and M. Yanai, 1980: Upper tropospheric waves in the tropics. Part I: Dynamical analysis in the wavenumber–frequency domain. *J. Atmos. Sci.,* **37,** 283–298.